Grazing-Incidence X-ray Diffraction Study of Octadecanoic Acid Monolayers

I. R. Peterson,*,†,‡,§ G. Brezesinski,†,|| B. Struth,† and E. Scalas†,⊥

Institut für Physikalische Chemie, Johannes Gutenberg-Universität, Jakob Welder-Weg 11, D-55099 Mainz, Germany, Max-Planck-Institut für Kolloid und Grenzflächenforschung, Rudower Chaussee 5, D-12489 Berlin, Germany, Centre for Molecular and Biomolecular Electronics, Coventry University, Priory Street, Coventry CV1 5FB, United Kingdom, Nima Technology, The Science Park, Coventry CV4 7EZ, United Kingdom, and Dipartimento di Fisica, Università di Genova, Via Dodecaneso 33, I-16146 Genova, Italy

Received: April 21, 1998; In Final Form: July 13, 1998

We report the observation of X-ray scattering profiles from monolayers of octadecanoic acid in the vicinity of room temperature and evidence for the existence near room temperature of all four hexatic rotator phases L_{2d}, Ov, L'_1, and LS, which differ in the details of their molecular tilt. While the incontrovertible triple-reflection signature of the chiral L'_1 phase was not observed, we propose that the previously reported rapid annealing behavior in this phase can lead to the disappearance of one, and in some cases two, of the three peaks.

Introduction

Monolayers of amphiphiles at aqueous interfaces play important roles in the stabilization of colloids, the cleansing action of detergents, the self-assembly properties of biological membranes, and the fabrication of Langmuir−Blodgett films. In fundamental investigations of the structure and thermodynamics of systems of low dimensionality, they provide systems that are experimentally readily accessible. Monolayers of this sort have been studied scientifically since the end of last century, when Pockels reported the isothermal thermodynamic behavior of octadecanoic (stearic) acid.[1] Since then, octadecanoic acid has been the subject of many monolayer investigations using such isotherm methods[2,3] and can be said without exaggeration to have been the workhorse material for monolayer and Langmuir−Blodgett studies.

For most of this period, isotherm measurement was essentially the only technique available for such investigations, which led to the wide recognition of four phases, called gas, liquid-expanded, liquid-condensed, and solid. Recently, our understanding of the structure of amphiphilic monolayers on water has been revolutionized by the advent of a number of new techniques, including fluorescence microscopy, Brewster angle microscopy (BAM), X-ray reflectivity, and grazing-incidence X-ray diffraction (GID), each of which is sensitive to aspects of the structure of the infinitesimal quantity of material in the surface monolayer. Of these, the X-ray diffraction techniques arguably provide the most detailed information about the monolayer structure, yielding quantitative data about the relationship of the molecules to their neighbors in the layer and to the adjoining bulk phases.

At room temperature, the isotherm of octadecanoic acid shows three of the four accepted phases (gas, liquid-condensed, and solid), and it is essentially independent of temperature over the whole of the accessible range. This property is consistent with the belief, widely held for many decades, that variations of monolayer behavior with temperature are of little interest and that the whole of the phase behavior can be accessed by changing the surface pressure. The transition to the nearly vertical 'solid' portion of the isotherm occurs at 26 mN/m, apart from systematic variations between different research groups of the order of 1 mN/m. The isotherm within the liquid-condensed region is nearly straight, with no hint of any change of organization. However, the new techniques have shown that the behavior of related monolayers is much richer and that the terms 'liquid-condensed' and 'solid' are misnomers. The differences in compressibility are not due to differences in crystallinity; in both regions the monolayer is hexatic[4,5] and thus shows characteristics of both solids and liquids. Instead, the compressibility differences are due to the presence or absence of molecular tilt,[6−8] and the 26 mN/m feature is a tilting transition. Each term describes not one phase, but a region containing several distinct phases. The 'liquid-condensed' region at room temperature has been shown using BAM to include at least two phases,[9,10] now symbolized L_{2d}[11,12] and Ov. The transition between them is recognized in BAM from the characteristic movements of domain walls. At different temperatures and for different chain lengths, the 'solid phase' can be one of at least three[13] and possibly four[14] phases. Octadecanoic monolayers at room temperature are in the high-temperature LS (LS_{II}) phase, while only the low-temperature CS phase is a true crystalline solid.

The absence of tilt in the LS phase and its presence in the L_{2d} and Ov phases have been most convincingly demonstrated by GID studies of other fatty acids. GID also reveals other details of the molecular packing. L_{2d} and Ov are distinguished by the tilt direction of the molecules with respect to their neighbors in the hexatic lattice, their nearest neighbor (NN) and their next-nearest neighbor (NNN), respectively,[15] so that the molecules can be considered to 'swivel' at the transition between them. However, these studies have not yet been carried out on octadecanoic acid itself. The present study aims to rectify this

† Johannes Gutenberg-Universität.
‡ Coventry University.
§ Nima Technology.
|| Max-Planck-Institut für Kolloid und Grenzflächenforschung.
⊥ Università di Genova.

10.1021/jp981941p CCC: $15.00
Published on Web 11/03/1998

oversight and to verify that, despite revealing no hint of their separate existence under constant investigation for over a whole century, these distinct phases and their characteristic molecular packings also occur in octadecanoic acid.

There was also a second aim related to the question of chirality. Both NN and NNN are directions of mirror symmetry of a two-dimensional hexatic lattice. When the molecules tilt along one of them, it remains as a direction of mirror symmetry of the whole phase. All three phases, LS, L_{2d}, and Ov, can therefore be superimposed on their mirror images. An interesting aspect of the present study is the question of the existence of a phase transitional between the latter two in which the molecular tilt is in a direction intermediate between the two symmetrical tilt directions. Despite the plane of mirror symmetry of each individual molecule in the monolayer, this L'_1 phase cannot be superimposed on its mirror image and hence is chiral. Since there are no symmetries to cause diffraction peaks to overlap in a powder pattern, the unequivocal signature of a chiral phase is the observation of three distinct powder reflections. A chiral rotator phase of monolayers has been predicted theoretically.[16]

Unequivocal evidence for a chiral rotator phase in monolayers has not yet been presented, even though a phase showing essentially identical packing is known in the alkanes[17] (R_{III}) and hydrated phospholipids[18] ($L_{\beta L}$). The L'_1 phase has been reported in a GID investigation of eicosanoic acid monolayers,[19] and a chiral herringbone phase has also been reported,[20] but other authors have either not observed a triple-peak phase at all or not reproducibly. In the GID study of eicosanoic acid, it was observed in the range of surface pressures corresponding to the Ov phase but at slightly lower temperatures. The earliest report of its existence in monolayers[21] may be erroneous. This was an isotherm miscibility study of the C22 acid and ethyl ester. New BAM observations[22] do not find L'_1 in the pure ethyl ester because, as the ester concentration increases, the pressure of the swivel transition decreases until it vanishes below the transition to the gas phase.

In the vast majority of known lamellar packings of long-chain compounds, the chains are all parallel with six nearest neighbors and are only slightly distorted from a hexagonal close packing (hcp).[23,24] Some recent publications have introduced the parameters ξ and ω, which describe the magnitude and direction of the distortion of a general two-dimensional Bravais lattice and which vanish in the hexagonal case.[19,25,26] These are a refinement of the Sirota distortion parameters,[17] and for describing monolayer packings, are preferable to standard crystallographic notation because they vary continuously and are unique yet allow the symmetry to be readily determined. Compared to the formulas presented in refs 25 and 26 for calculating ξ and ω from the measured scattering vector moduli of the powder pattern peaks (either 2D in the plane of the water surface or 3D, those for degenerate peaks repeated), the following formula has been found to be both simpler and better conditioned:

$$\xi e^{2i\omega} = 2\frac{\sum r_n^2 e^{2\pi i n/3}}{\sum r_n^2}$$

Experimental Section

The present measurements were made over a 24 h period on Beamline BW1 at HASYLAB, DESY, Hamburg, Germany. The measurement setup has been described previously.[27] Octadecanoic (stearic) acid (>99% pure) was purchased from Aldrich and made up into approximately 1 mM spreading solutions using P.A. grade chloroform from Merck. The subphase was in all cases ultrapure water prepared using a Millipore desktop unit immediately before use.

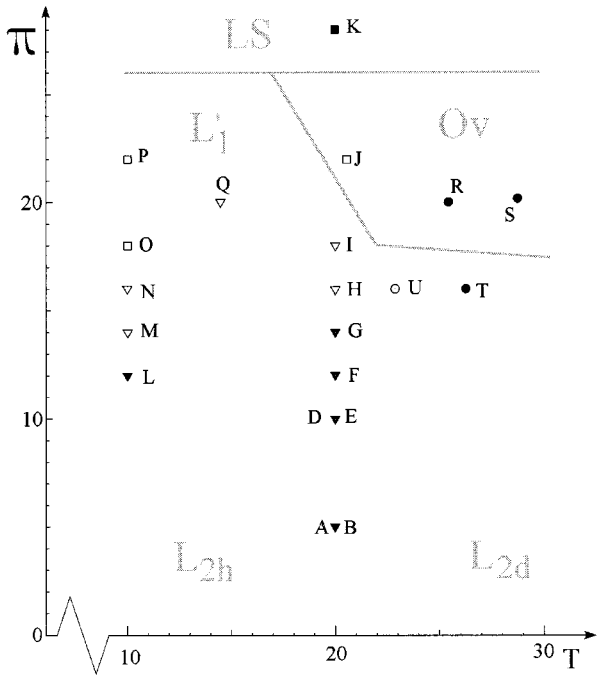

Figure 1. π vs T diagram showing as points the surface conditions of the different measurement sets. The dotted line shows the phase boundaries reported by Overbeck and Möbius. The symbols represent qualitatively different diffraction patterns as follows: triangles, two peaks with Q_z's approximately in the ratio 0:1; circles, two peaks with Q_z's approximately in the ratio 1:2; squares, one peak; filled, consistent with monolayer powder pattern; unfilled, inconsistent with monolayer powder pattern.

A monolayer was spread at the beginning of the measurement period, and then a second one was added after approximately 18 h. A hydrophilic borosilicate slab under the monolayer damped capillary waves induced by mechanical vibrations. The horizontally propagating fan beam from the synchrotron was monochromated to a wavelength of 1.3639 Å, confined vertically using slits so as to illuminate approximately half the trough width, and deflected downward using a beryllium crystal in a transmission (Laue) diffraction configuration. At regular intervals, the vertical position of the trough was adjusted so as to center the beam laterally, and if the specular reflectivity fell below 0.96, the water level relative to the glass block was adjusted.

The trough was moved horizontally every few hours to expose new areas of the monolayer to the beam. The horizontal distribution of the diffracted X-rays was determined by scanning a Soller collimator (consisting of many parallel vertical plates), and their vertical distribution was determined using a vertically resolving linear position-sensitive detector mounted behind the Soller collimator in the plane of incidence and normal to the line joining the center of the beam footprint on the water surface and the detector center.[28] The accumulated position-resolved counts were corrected for polarization, footprint, powder-averaging (Lorentz factor), and distance effects. The Yoneda−Vineyard peak[29] was used to determine the detector position corresponding to the waterline, but otherwise, all values within twice the angle of total external reflection were discarded.

The whole set of corrected intensities was least-squares fitted to a sum of model peaks paired symmetrically above and below the plane of the water surface plus a linear background. Each

TABLE 1: Best-Fit Parameters for All Peaks Observed at the Surface Conditions of Temperature, *T*, and Surface Pressure, π, Investigated: Peak Intensity, *I*, Peak Coordinates, Q_{xy} and Q_z, and Their Full Widths at Half Maximum

set	*T*, °C	π, mN/m	*I*, arb unit	Q_{xy}, rad Å^{-1}	Q_z, rad Å^{-1}	ΔQ_{xy}, (FWHM), rad Å^{-1}	ΔQ_z, (FWHM), rad Å^{-1}	χ^2
A/B	20	5	126.8	1.481	0.000	0.020	0.314	1.337
			107.1	1.403	0.634	0.039	0.290	
D/E	20	10	50.276	1.470	0.000	0.020	0.320	8.98
			130.5	1.436	0.525	0.037	0.404	
F	20	12	109.6	1.494	0.000	0.025	0.304	1.276
			143.1	1.454	0.495	0.037	0.297	
G	20	14	103.7	1.498	0.000	0.027	0.322	1.120
			148.6	1.468	0.440	0.037	0.291	
H	20	16	101	1.504	0.000	0.028	0.319	1.182
			165	1.482	0.379	0.035	0.285	
I	20	18	125	1.503	0.065	0.026	0.284	1.186
			165	1.481	0.379	0.033	0.275	
J	20.4	22	308	1.522	0.059	0.041	0.268	1.718
K	20	28	299	1.522	0.000	0.038	0.298	1.616
L	9.8	12	76.5	1.486	0.000	0.031	0.286	1.149
			138	1.477	0.485	0.059	0.297	
M	10	14	62.5	1.495	0.000	0.036	0.279	1.100
			143	1.495	0.395	0.058	0.300	
N	10	16	11.4	1.492	0.000	0.046	0.233	1.134
			154	1.511	0.249	0.060	0.346	
O	10	18	225	1.524	0.117	0.067	0.280	1.254
P	10	22	212	1.532	0.002	0.077	0.274	1.237
Q	14.5	20	99	1.512	0.020	0.045	0.439	1.107
			95	1.507	0.292	0.057	0.026	
R	25.4	20	220	1.500	0.190	0.020	0.283	1.228
			112	1.477	0.381	0.030	0.261	
S	28.7	20	226	1.496	0.194	0.020	0.295	1.336
			126	1.471	0.387	0.028	0.270	
T	26.3	16	209	1.485	0.246	0.023	0.287	1.330
			85.6	1.448	0.492	0.049	0.331	
U	22.9	16	174	1.495	0.207	0.027	0.317	1.219
			83.9	1.469	0.413	0.044	0.305	

model peak was Lorentzian parallel to the water and Gaussian normal to it.[15] For the phases identified as NN or NNN tilted, the variations of the *z*-wavevector components of the two peaks during the Marquardt least-squares fit algorithm were restricted to either $Q_{z2} = 0$ or $Q_{z1} = 2Q_{z2}$, respectively.[25]

Results

The 18 different surface conditions of surface pressure π and temperature *T* at which extensive scans of the scattered intensity were taken are shown in graphical form in Figure 1. The symbols marking each surface condition are an attempt to categorize the qualitative features of the present diffraction patterns. The shaded lines on this figure show the positions of phase transitions observed using BAM. The best-fit parameters for each of the diffraction peaks observed in the present investigation are listed in Table 1.

Figure 2 shows the pattern for data set L. It has two peaks, one out of and one in the plane of the water surface. Their Q_z's are in the ratio 0:1, corresponding exactly to the expectations for the L_{2d} phase (NN tilt). There were five measurement sets that were unequivocally of this sort (A/B, D/E, F, G, and L), all corresponding to surface pressures π less than 15 mN/m, and they are all represented in Figure 1 by filled triangles.

Figure 3 shows the pattern for data set T. It has two peaks out of the plane of the water surface with Q_z's in the ratio 1:2, corresponding exactly to the expectations for the Ov phase (NNN tilt). There were three measurement sets unequivocally of this sort (R, S, and T), all with π greater than 15 mN/m and *T* greater than 22 °C, and they are all represented in Figure 1 by filled circles.

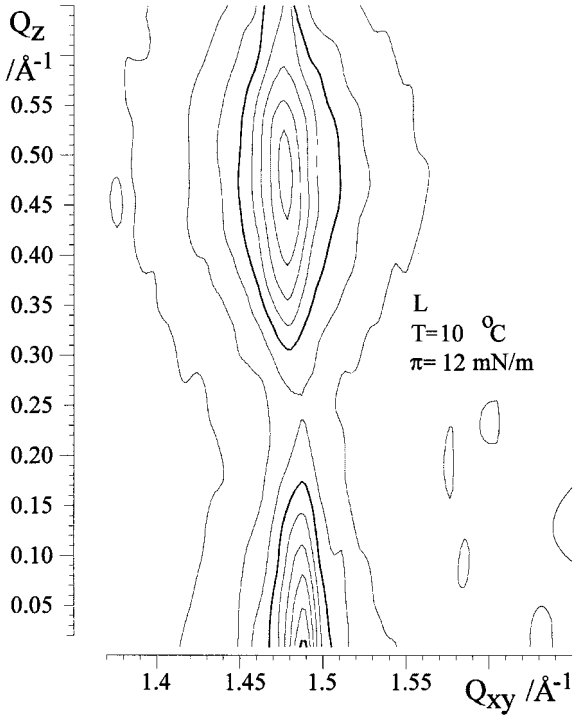

Figure 2. Contour plot, for the measurement set L (10 °C, 12 mN/m), of the corrected diffraction intensity versus in-plane and out-of-plane scattering vector components Q_{xy} and Q_z (rad Å^{-1}).

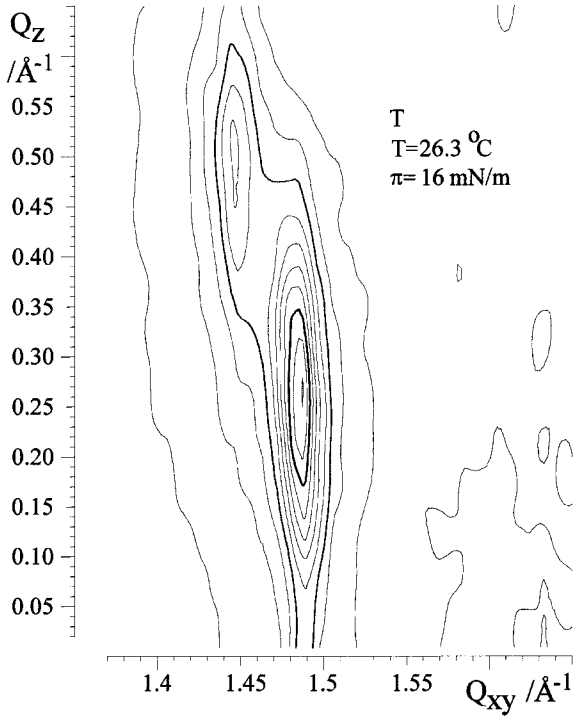

Figure 3. Contour plot, for the measurement set T (26.3 °C, 16 mN/m), of the corrected diffraction intensity versus in-plane and out-of-plane scattering vector components Q_{xy} and Q_z (rad Å^{-1}).

One data set, K, had only one peak in the plane of the water surface. Since it corresponds to a surface pressure of 28 mN/m, above the well-documented tilt transition, it may be assigned unequivocally to the upright hexagonal LS phase and is represented in Figure 1 by a filled square.

The remaining data sets all present anomalies that cannot be explained by errors of measurement of either the diffraction pattern or the surface conditions. Figure 4 shows a sequence

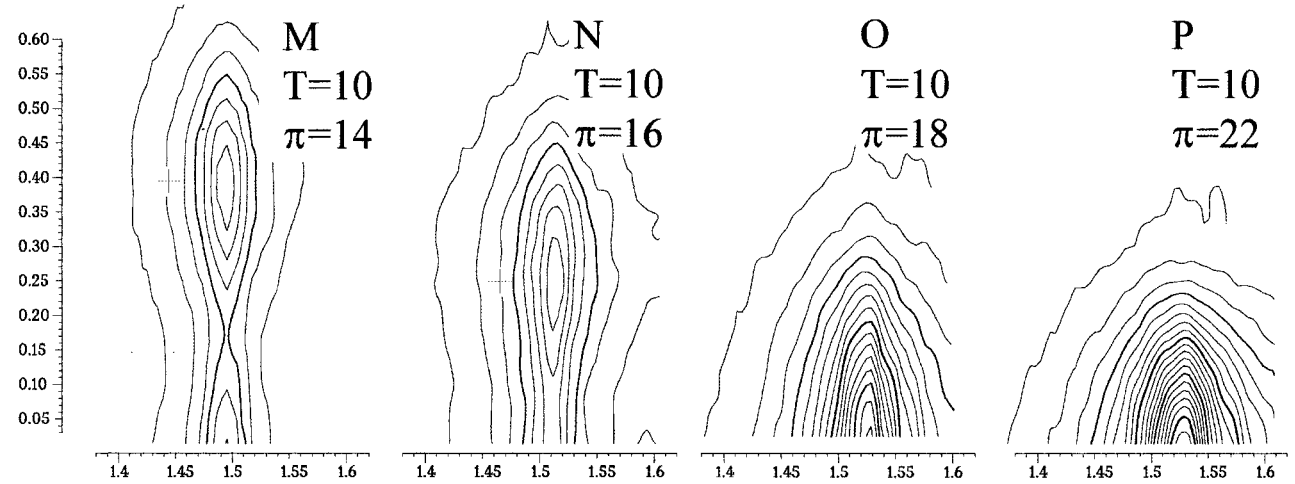

Figure 4. Sequence of contour plots of the corrected diffraction intensity at 10 °C as the surface pressure is increased from 14 to 22 mN/m.

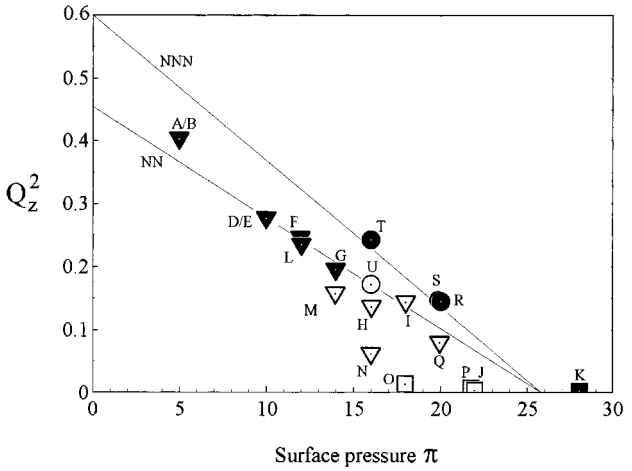

Figure 5. Plot of $(Q_z^{max})^2$ versus surface pressure π for all measurement sets. The two lines are the best-fit loci expected for the NNN-tilted (upper) and NN-tilted (lower) phases, respectively.

of four contour plots of corrected intensity at 10 °C as the surface pressure is increased from 14 mN/m to 22 mN/m. When π is increased from 14 mN/m to 16 mN/m, the pattern remains qualitatively similar but the in-plane Q's for the two peaks increase by 0.05 while the value of Q_z for the out-of-plane peak decreases by almost a factor of 2. At 18 and 22 mN/m, despite being in both cases significantly below the known pressure of the tilting transition, only one diffraction peak is visible and it is essentially in the plane of the water surface. From the BAM observations, the molecules are known to be tilted at these pressures and this must give rise to an out-of-plane reflection in the powder pattern.

Anomalies are also apparent in Figure 5, which shows the values of the square of the maximum value of Q_z plotted against surface pressure π for all the data sets. The interpretation of this plot for octadecanoic acid is especially simple because the surface pressure of its tilt transition is essentially independent of temperature. It is expected that the packing normal to the chains is almost hexagonal, with a chain cross section of 0.20 nm^2. Hence, in reciprocal space, all the reflections lie equally spaced around the circumference of a disk whose angle θ of inclination to the water surface is the tilt angle of the monolayer molecules. The value of $\sin^2\theta$ is expected to vary linearly with surface pressure, with a gradient not strongly dependent on temperature, and the same for both NN and NNN phases. Hence, all points in Figure 5 should lie on one of two straight lines intersecting at the point (26, 0) and with gradients in the ratio 3:4. The points for the one-peak sets, J, O, and P, and for the two-peak sets, H, I, M, N, Q, and U, all lie significantly below the line expected for the closest symmetrical tilt possibility.

TABLE 2: Lattice and Tilt Parameters Extracted from Table 1 for All Surface Conditions Compatible with Symmetrical Tilt

measurement set	surface conditions T	surface conditions π	symmetry azimuth	chain cross section, A'	chain tilt, θ	distortion (chain normal), ξ'
A/B	20	5	NN	19.75	28.01	0.051
D/E	20	10	NN	20.03	23.05	0.052
F	20	12	NN	19.69	21.64	0.037
G	20	14	NN	19.71	19.21	0.030
H	20	16	NN	19.71	16.52	0.022
L	9.8	12	NN	19.46	20.80	0.059
R	25.4	20	NNN	19.82	14.46	0.012
S	28.7	20	NNN	20.00	18.65	0.013
T	26.3	16	NNN	19.91	18.76	0.021

Since it only takes five parameters to define a two-dimensional lattice of tilted rods, it is only necessary to complement the anomalous two-peak sets with one additional value to deduce the position of the third peak. In Figure 4, this position has been deduced for data sets M and N and indicated by crosses on the contour plots by extrapolating the in-plane cross-sectional area from the other two phases and using the fact that none of the transitions are visible in isotherms. In both cases, the crosses are in similar positions relative to the peaks previously reported for the chiral phase of eicosanoic acid.[19] The small value of χ^2 indicates that the third peak must be considerably less intense than the other two. In the case of the one-peak anomalous data sets, this procedure is not possible.

Table 2 shows the distortion parameters extracted from the peak coordinates given in Table 1. In the case of the data sets A−H, K, L, and R−T, this is straightforward and all five lattice parameters can be extracted from the six measured parameters. For the anomalous two-peak sets I, M, N, Q, and U, the four measured parameters were complemented by an interpolated value of in-plane area.

Discussion

Hexatics, first predicted theoretically by Nelson and Halperin,[30,31] are phases with local crystalline order giving rise to distinct diffraction reflections resembling those of a crystal[32,33] but in which this order is perturbed by a finite density of lattice defects in thermodynamic equilibrium that destroy long-range order.

In all recent GID studies of amphiphilic monolayers in which diffraction peaks were observed, it has been assumed that the coordination number is six, as is the case for most aliphatic chain derivatives.[23] The present results are consistent with this idea. The vertical peak widths are always approximately equal to 0.3 rad $Å^{-1}$, implying a correlation length in the *z* direction of 20 Å. This is essentially equal to the thickness of the monolayer, indicating that the molecules are behaving like rigid rods and that the crystallinity giving rise to the peaks is not restricted to the vicinity of the carboxylic headgroups. In the general case, a lattice with 6-fold coordination gives rise to three low-order peaks. Normally, all domain orientations are represented in the footprint, because domain diameters in monolayers[34] are normally 100 μm, compared to an X-ray beam footprint on the order of 50 mm. For any possible reflection with *d* spacing greater than the observing wavelength, there are two orientations that will bring it onto the Ewald sphere. Hence, in a powder pattern, all reflections are present in the diffraction pattern without taking any special precautions. However, symmetries of the lattice may reduce the number of distinct powder-pattern reflections to two, or even one, by causing them to become degenerate, i.e., to overlap perfectly.

All the observed peaks have an appreciable in-plane width ΔQ_{xy}. Although an ideal crystal in two dimensions does not have true long-range order, rather only quasi-long-range order, leading to power−law profile diffraction peaks instead of δ functions, the FHWM of its peaks should still be essentially equal to the diffractometer resolution. This has been found to be the case in the CS phase, which is not accessible in octadecanoic acid monolayers; extrapolation from its ranges of stability in longer chain amphiphiles suggests that it is stable below 0 °C and therefore unobservable as a result of subphase freezing. Peak broadening is often interpreted as arising from a polycrystalline texture. On this interpretation, the average domain size is extremely small, on the order of tens of lattice spacings. However, it is known from optical data that domain sizes are much larger, on the order of 100 μm, and that the crystal orientation may vary continuously within the domains. This behavior is characteristic for hexatic mesophases.

In data sets J, O, and P, the single peak is in or close to the water surface but the surface pressure is signficantly lower than that of the tilting transition and the value of Q_z is lower than would be expected from extrapolation from the L_{2d} phase. The sets H, I, M, N, and Q each show two reflections, but again the value of Q_z^{max} is unexpectedly low. All of these observations are inconsistent with the present understanding of monolayer powder patterns.[25] In each case, there must be an additional peak or peaks that are not visible in the diffraction pattern. This is only physically possible if the monolayer lattice does not take on all possible orientations over the 50 mm long footprint of the X-ray beam. The characteristic size of monolayer domains must therefore have increased by approximately 2 orders of magnitude within an hour.

This conclusion is consistent with the identification of this region of surface pressure and temperature as the range of stability of the rapid-annealing phase reported in studies of topological defects in docosanoic acid by Bibo et al.[35] On the *T* vs π diagram, the relationship to the Ov and L_{2d} phases is the same as that observed for the triple-reflection phase in a GID study of eicosanoic acid by Peterson et al.[19]

Our use, during the measurement session, of a borosilicate glass block to dampen waves is less than ideal, because when the subphase water is stored in contact with such glass, long time-constant relaxations of the monolayer structure have been reported.[36,37] These are believed to be related to the strong affinity of carboxylic monolayers for ppb concentrations of certain metal ions.[38] Its employment was dictated by availability at the time. However, in the present experiments, the monolayer was left on the water surface for at most 18 h and then respread.

It should be noted that none of the phases reported here are dense packed in the sense of Kitaigorodskii.[24] In addition to the well-known crystalline triclinic and orthorhombic packings with chain cross sections of 0.182 and 0.1835 nm^2, respectively, packings with a local chain cross section as low as 0.17 nm^2 have been recently discovered.[39]

Conclusion

The present investigation has confirmed that the rich phase behavior reported for related amphiphiles also applies to octadecanoic acid. Four phases have been observed at readily accessible surface pressures and in the immediate vicinity of room temperature.

The Overbeck−Möbius phase occurs in the high-temperature high-pressure part of the liquid-condensed region. As already confirmed by Dutta et al. and Peterson et al. in related systems, the molecules in this phase are tilted toward their next-nearest neighbor. Over the whole of the low-pressure region, the molecules tilt toward their nearest neighbor.

Despite the absence of the characteristic powder pattern for the chiral phase showing three distinct reflections, it is possible to deduce its presence under at least seven of the present measurement conditions. Conclusive observation in the future would require a measurement configuration in which the trough can be rotated or the subphase stirred.

Acknowledgment. The authors thank Dr. K. Kjaer for assistance with the measurements, Dr. V. M. Kaganer, Prof. C. M. Knobler, Prof. P. S. Pershan, and Prof. H. Möhwald for useful discussions, and HASYLAB at DESY, Hamburg, Germany, for synchrotron beam time.

References and Notes

(1) Pockels, A. *Nature* **1891**, *43*, 437.
(2) Gaines, G. L., Jr. *Insoluble Monolayers at Liquid−Gas Interfaces*; Wiley-Interscience: New York, 1966; pp 165, 187.
(3) Mingotaud, A. F.; Mingotaud, C.; Patterson, L. K. *Handbook of Monolayers*; Academic: San Diego, 1993.
(4) Peterson, I. R. *Br. Polym. J.* **1987**, *19*, 391.
(5) Fischer, T. M.; Bruinsma, R.; Knobler, C. M. *Phys. Rev. E* **1994**, *50*, 413.
(6) Kaganer, V. M.; Osipov, M. A.; Peterson, I. R. *J. Chem. Phys.* **1993**, *98*, 3512.
(7) Kenn, R. M.; Böhm, C.; Bibo, A. M.; Peterson, I. R.; Kjaer, K.; Als-Nielsen, J. *J. Phys. Chem.* **1991**, *95*, 5, 2092.
(8) Lin, B.; Shih, M. C.; Bohanon, T. M.; Ice, G. E.; Dutta, P. *Phys. Rev. Lett.* **1990**, *65*, 191.
(9) Overbeck, G. A.; Möbius, D. *J. Phys. Chem.* **1993**, *97*, 7999.
(10) Ruiz-Garcia, J.; Qiu, X.; Tsao, M. W.; Marshall, G.; Knobler, C. M.; Overbeck, G. A.; Möbius, D. *J. Phys. Chem.* **1993**, *97*, 6955.
(11) Kaganer, V. M.; Indenbom, V. L. *J. Phys. II* **1993**, *3*, 813.
(12) Kaganer, V. M.; Loginov, E. B. *Phys. Rev. Lett.* **1993**, *71*, 2599.
(13) Ställberg-Stenhagen, S.; Stenhagen, E. *Nature* **1945**, *156*, 239.
(14) Shih, M. C.; Bohanon, T. M.; Mikrut, J. M.; Zschack, P.; Dutta, P. *Phys. Rev. A* **1992**, *45*, 5734.
(15) Durbin, M.; Malik, A.; Ghaskadvi, R.; Shih, M. C.; Zschack, P.; Dutta, P. *J. Phys. Chem.* **1994**, *98*, 1753.
(16) Selinger, J. V.; Nelson, D. R. *Phys. Rev. Lett.* **1988**, *61*, 416.
(17) Sirota, E. B.; King, H. E., Jr.; Singer, D. M.; Shao, H. H. *J. Chem. Phys.* **1993**, *98*, 5809.
(18) Smith, G. S.; Sirota, E. B.; Safinya, C. R.; Plano, R. J.; Clark, N. A. *J. Chem. Phys.* **1990**, *92*, 4519.
(19) Peterson, I. R.; Kenn, R. M.; Goudot, A.; Fontaine, P.; Rondelez, F.; Bouwman, W. G.; Kjaer, K. *Phys. Rev. E* **1996**, *53*, 667.
(20) Durbin, K.; Malik, A.; Richter, A. G.; Ghaskadvi, R.; Gog, T.; Dutta, P. *J. Chem. Phys.* **1997**, *106*, 8216.
(21) Bibo, A. M.; Knobler, C. M.; Peterson, I. R. *J. Phys. Chem.* **1991**, *95*, 5591.

(22) Teer, E.; Knobler, C. M.; Lautz, C.; Wurlitzer, S.; Kildae, J.; Fischer, T. M. *J. Chem. Phys.* **1997**, *106*, 1913.
(23) Segerman, E. *Acta Crystallogr.* **1965**, *19*, 789.
(24) Kitaigorodskii, A. I. *Organic Chemical Crystallography*; Consultants Bureau: New York, 1961.
(25) Kaganer, V. M.; Peterson, I. R.; Kenn, R. M.; Shih, M. C.; Durbin, M.; Dutta, P. *J. Chem. Phys.* **1995**, *102*, 9412.
(26) Peterson, I. R.; Kenn, R. M. *Langmuir* **1994**, *10*, 4645.
(27) Kjaer, K. *Experimental stations at HASYLAB*; Risø National Laboratory, 1994; pp 88−89.
(28) Leveiller, F.; Jacquemain, D.; Leiserowitz, L.; Kjaer, K.; Als-Nielsen, J. *J. Phys. Chem.* **1992**, *96*, 10380.
(29) Sinha, S. K.; Sirota, E. B.; Garoff, S.; Stanley, H. B. *Phys. Rev. B* **1988**, *38*, 2297.
(30) Nelson, D. R.; Halperin, B. I. *Phys. Rev. B* **1979**, *19*, 2457.
(31) Nelson, D. R.; Halperin, B. I. *Phys. Rev. B* **1980**, *21*, 5212.
(32) Aeppli, G.; Bruinsma, R. *Phys. Rev. Lett.* **1984**, *53*, 2133.
(33) Peterson, I. R.; Kaganer, V. M. *Phys. Rev. Lett.* **1994**, *73*, 102.
(34) Veale, G.; Girling, I. R.; Peterson, I. R. *Thin Solid Films* **1985**, *127*, 293.
(35) Bibo, A. M.; Peterson, I. R. *Thin Solid Films* **1992**, *210*, 515.
(36) Albrecht, O. *Thin Solid Films* **1983**, *99*, 227.
(37) Schwartz, D. K.; Schlossman, M. L.; Pershan, P. S. *J. Chem. Phys.* **1992**, *96*, 2356.
(38) Langmuir, I.; Schaeffer, V. J. *J. Am. Chem. Soc.* **1937**, *59*, 2400.
(39) Silver, J.; Martin, S.; Marsh, P. J.; Frampton, C. S. *Acta Crystallogr., Sect. C* **1996**, *52*, 1261.